Monatshefte für Chemie 115, 1013—1038 (1984)

Monatshefte für Chemie
Chemical Monthly

Physical Adsorption of Gases on Energetically Heterogeneous Solids II. Theoretical Extension of a Generalized *Langmuir* Equation and Its Application for Analysing Adsorption Data

Mieczysław Jaroniec and **Adam W. Marczewski**

Institute of Chemistry, M. Curie-Skłodowska University, PL-20031 Lublin, Poland

(Received 21 February 1984. Accepted 19 March 1984)

The generalized *Langmuir* equation proposed in part I is extended to monolayer adsorption with lateral interactions and to multilayer adsorption on heterogeneous surfaces with random distribution of adsorption sites. New differential functions, useful for interpreting the adsorption data, are introduced to study the mathematical and physical properties of this equation. These functions are applied to study three gas adsorption systems available from the literature.

(Keywords: Gas adsorption; Multilayer adsorption; Adsorption data analysis; Heterogeneous solids)

Gasadsorption auf energetisch heterogenen Feststoffen, 2. Mitt.: Die theoretische Erweiterung einer generalisierten Langmuir-Gleichung und ihre Anwendung zur Analyse von Adsorptionsdaten

Die generalisierte *Langmuir*-Gleichung, die in der 1. Mitt. beschrieben wurde, wird für die einlagige Adsorption mit lateralen Wechselwirkungen und für die viellagige Adsorption auf heterogenen Oberflächen mit einer Zufallsverteilung von Adsorptionsplätzen erweitert. Es werden neue Differentialfunktionen zur Untersuchung der mathematischen und physikalischen Eigenschaften dieser Gleichung eingeführt, die sich als fruchtbringend zur Interpretation von Adsorptionsdaten erweisen. Diese Funktionen werden zur Untersuchung von drei Gasadsorptionssystemen aus der Literatur herangezogen.

Introduction

In the preceding paper[1] a new equation for the overall gas adsorption isotherm has been proposed. It is analogous to the empirical equation

introduced for describing the single-solute adsorption from dilute solutions[2]. The above equation has been derived by solving the fundamental integral equation for the *Langmuir* local isotherm and three parameter quasi-*Gauss*ian energy distribution. It has been called the generalized *Langmuir* equation (G*L*E). Its mathematical form may be expressed as follows:

$$\theta_t(p) = \left[\frac{(\bar{K}p)^n}{1+(\bar{K}p)^n}\right]^{m/n} \tag{1}$$

where θ_t is the relative coverage of a heterogeneous surface; p is the adsorbate pressure; $\bar{K}$ is the constant analogous to the *Langmuir* constant; m and n are heterogeneity parameters. The relative coverage θ_t is defined as the ratio of the adsorbed amount a by the monolayer surface coverage a_0. The constant $\bar{K}$ is defined as follows[1]:

$$\bar{K} = K_0 \exp(\varepsilon_0/RT) \tag{2}$$

where K_0 is the pre-exponential factor and ε_0 is the "characteristic" adsorption energy for a given distribution function, which determines its position on the energy axis. The heterogeneity parameters m and n may change from zero to unity. For $m = n$ the energy distribution, corresponding to Eq. (1), is symmetrical, however, for $m \neq n$ it is asymmetrical. If $m > n$ it is widened on the left-hand side, however for $m < n$ it is widened on the right-hand side. The mathematical properties of Eq. (1) and its energy distribution function were discussed in details in the preceding paper[1].

Eq. (1) comprises three main isotherm equations known in the theory of adsorption on heterogeneous surfaces. For $m = n$ Eq. (1) becomes the *Langmuir-Freundlich* equation (*LF*E), for $m = 1$ and $n \in (0,1)$ it reduces to the *Tóth* equation (*T*E), however, for $m \in (0,1)$ and $n = 1$ it reduces to the generalized *Freundlich* equation (G*F*E). Eq. (1) and its special cases are reducible to the *Langmuir* equation when the heterogeneity parameters become equal to unity[1]. Eq. (1) describes the monolayer localized adsorption of gases without lateral attractive interactions in the surface phase.

In this paper Eq. (1) will be extended to the monolayer adsorption with lateral attractive interactions on energetically heterogeneous solids showing random topography distribution of adsorption sites on the solid surface. Moreover, we shall generalize Eq. (1) to take into account the multilayer effects according to the *BET* adsorption model. The new functions, useful for interpreting the adsorption data, will be also introduced to study the mathematical and physical behaviour of Eq. (1)

and its modified forms. Finally, three gas adsorption systems will be examined by means of Eq. (1) to show its utility for analysing the experimental adsorption data.

Results and Discussion

Extension of Eq. (1) for Fowler-Guggenheim and BET Local Isotherms

In the review[3] a method for generalizing the single-gas adsorption isotherms without lateral interactions to the isotherm equations describing adsorption with lateral interactions is discussed. This method transforms the overall adsorption isotherms derived for the *Langmuir* local behaviour to the overall isotherm equations being an extension of the *Fowler-Guggenheim* local isotherm. One limitation of this method is connected with the topography of adsorption sites on the surface; it may be used only to the heterogeneous surfaces showing random distribution of adsorption sites. Extending Eq. (1) according to the above method, we have:

$$\theta_t(p) = \left\{ \frac{[\bar{K} p \exp(\alpha \theta_t)]^n}{1 + [\bar{K} p \exp(\alpha \theta_t)]^n} \right\}^{m/n} \tag{3}$$

where α is the parameter proportional to the interaction energy between two nearest neighbouring molecules in the monolayer. The isotherm Eq. (3) is denoted by α-G*L*E.

In the review[3] a procedure for extending the monolayer gas adsorption isotherms to the multilayer adsorption is also discussed. This procedure was firstly proposed by *Berezin* and *Kiselev*[4]. According to this procedure the pressure p in the monolayer gas adsorption isotherms is replaced by a function $h(x)$, where $x = p/p_s$ and p_s is a saturation vapour pressure, the monolayer relative coverage θ_t is replaced by $\theta_t^M/g(x)$ and $\bar{K}$ is replaced by $\bar{C} = \bar{K} p_s$. The symbol θ_t^M is the multilayer surface coverage and x is the relative pressure. The analytical forms of the functions $h(x)$ and $g(x)$ are dependent upon the multilayer local adsorption isotherm. For the *BET* classical adsorption isotherm (*BET* equation for the infinite number of adsorbed layers) with a great *BET* constant, the functions $h(x)$ and $g(x)$ are equal to:

$$h(x) = x \tag{4}$$

and

$$g(x) = 1/(1 - x) \tag{5}$$

However, for the full form of the *BET* classical isotherm the function $g(x)$ is given by Eq. (5), whereas the function

$$h(x) = x/(1 - x) \tag{6}$$

In the paper[5] the analytical expressions for the functions $h(x)$ and $g(x)$, corresponding to another forms of the *BET* equation, were discussed.

As an example, we present the extended from of Eq. (3) obtained by means of the functions $h(x)$ and $g(x)$ expressed by Eqs. (4) and (5):

$$\theta_t^M(1-x) = \left\{\frac{[\bar{C}x\exp(\alpha\,\theta_t^M(1-x))]^n}{1+[\bar{C}x\exp(\alpha\,(\theta_t^M(1-x))]^n}\right\}^{m/n} \tag{7}$$

For $\alpha = 0$ (adsorption without lateral interactions in the monolayer) Eq. (7) may be treated as an extended form of Eq. (1).

Mathematical Properties of the α-G*L*E

Firstly, we shall discuss the critical parameters of Eq. (3) (α-G*L*E). Calculating the second derivative $\partial^2 \ln p/\partial\theta_t^2$ for Eq. (3) and equating it to zero, we can evaluate the coordinates of the inflection point for the adsorption isotherm θ_t plotted as a function of $\ln p$. These coordinates are equal to:

$$\theta_t^{in} = [\nu/(1+\nu)]^\nu \tag{8}$$

and

$$p_{in} = \nu^{1/n}/\{\bar{K}\exp[\alpha\,(\nu/(1+\nu))^\nu]\} \tag{9}$$

where

$$\nu = m/n \tag{10}$$

However, calculating the first derivative $\partial \ln p/\partial\theta_t$ and the second derivative $\partial^2 \ln p/\partial\theta_t^2$ for Eq. (3) and equating these derivatives to zero, we can evaluate the critical parameters; they are:

$$\theta_t^{cr} = \theta_t^{in};\ p^{cr} = \nu^{1/n}/[\bar{K}\exp(1/m + 1/n)] \tag{11}$$

and

$$\alpha^{cr} = (1/m + 1/n)\cdot(1/\nu + 1)^\nu \tag{12}$$

The parameter ν may be called an "asymmetry" coefficient. For $\nu = 1$ (then $m = n$) the energy distribution corresponding to the G*L*E is symmetrical, however, for $\nu \neq 1$ it is asymmetrical with an expansion on the left-hand side ($m > n$) or on the right-hand side ($m < n$). For $\nu = 1$ (*LF*E) Eqs. (11) and (12) give: $\theta_t^{cr} = 0.5$ and $\alpha^{cr} = 4/n$; such a result has been obtained for the *LF*E by *Dubinin* et al.[6].

Fig. 1 presents the dependence of θ_t^{cr} vs. $\ln\nu$ (the dashed line) and $\ln\theta_t^{cr}$ vs. $\ln\nu$ (the solid line). These dependences are decreasing functions. Let us discuss the dependence of θ_t^{cr} vs. $\ln\nu$; the critical value of θ_t decreases from unity to $1/e$. For $n \gg m$ ($\nu \to 0$ and $\ln\nu \to -\infty$) the

critical coverage value θ_t^{cr} tends to unity; in this case the generalized *Freundlich* isotherm[7] is a bordering equation ($n = 1$ and m close to zero). An analogous dependence of θ_t^{cr} vs. m has been obtained for the generalized *Freundlich* equation in [8]. For $m = n$ we have $\theta_t^{cr} = 0.5$. However, for $m \gg n$ ($\nu \to \infty$ and $\ln \nu \to \infty$) the critical value of θ_t tends to $1/e$; in this case the *Tóth* isotherm[9] is a bordering equation ($m = 1$ and n close to zero). The dependences of p^{cr} and α^{cr} upon the heterogeneity parameters m and n are more complex than for θ_t^{cr}, which depends on the asymmetry coefficient only.

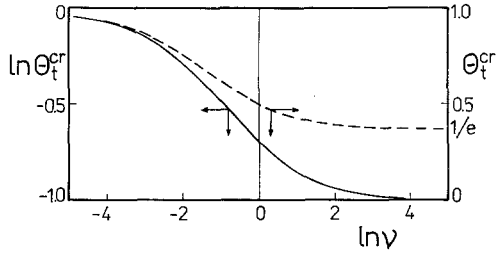

Fig. 1. Dependence of the critical coverage θ_t^{cr} upon the logarithm of the asymmetry coefficient ν (the dashed line) and $\ln\theta_t^{cr}$ vs. $\ln\nu$ (the solid line)

In practical applications of the α-G*L*E for describing the experimental data, functions φ, Φ and ψ_m are very useful; they are defined as follows:

$$\varphi = \frac{\partial \ln a}{\partial \ln p} \tag{13}$$

$$\psi_m = \ln|m/\varphi - 1| \tag{14}$$

and

$$\Phi = \ln\left|\frac{\partial(1/\varphi)}{\partial \ln p}\right| \tag{15}$$

In the case of Eq. (3) these functions are expressed by:

$$\varphi = \frac{m(1-\theta_t^{1/\nu})}{1 - m\alpha\theta_t(1-\theta_t^{1/\nu})} \tag{16}$$

$$\psi_m = \ln\left|\frac{\theta_t^{1/\nu}}{1-\theta_t^{1/\nu}} - m\alpha\theta_t\right| \tag{17}$$

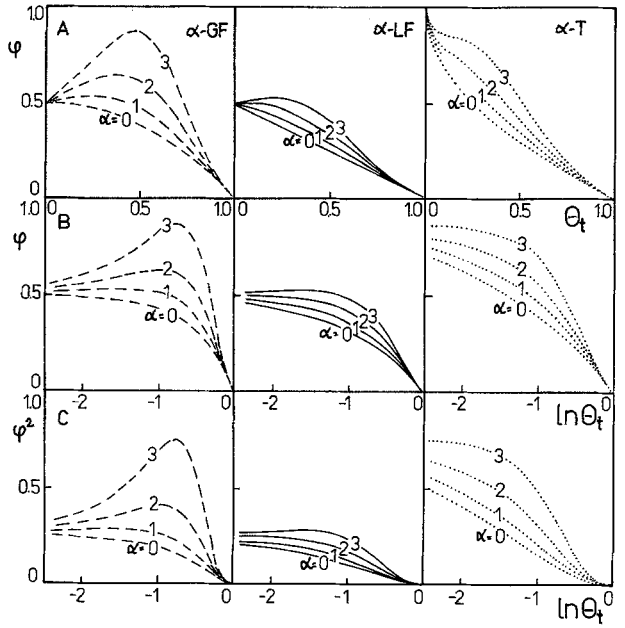

Fig. 2. Functions φ vs. θ_t (part A), φ vs. $\ln \theta_t$ (part B) and φ^2 vs. $\ln \theta_t$ (part C) for three special cases of α-G*L*E and different values of the parameter α. The calculations were made by using the parameters: $n = 1$ and $m = 0.5$ (α-G*F*E the dashed lines), $n = m = 0.5$ (α-*LFE* the solid lines) and $n = 0.5$ and $m = 1$ (α-*T*E the dotted lines)

and

$$\Phi = \ln \left| \frac{\frac{1}{\nu} \theta_t^{1/\nu}/(1 - \theta_t^{1/\nu}) - m\alpha\theta_t(1 - \theta_t^{1/\nu})}{1 - m\alpha\theta_t(1 - \theta_t^{1/\nu})} \right| \tag{18}$$

In Figs. 2–6 the model functions φ, ψ_m and Φ are presented for selected values of m and n. These functions have been calculated by assuming the characteristic values of m and n: $n = 1$ and $m = 0.5$ (the generalized *Freundlich* equation involving lateral interactions: α-G*F*E), $n = m = 0.5$ (α-*LFE*), $n = 0.5$ and $m = 1$ (α-*T*E).

Fig. 2 presents the function φ vs. θ_t and vs. $\ln \theta_t$ and the function φ^2 vs. $\ln \theta_t$ for the above three cases. For α-*LFE* and $\alpha = 0$ the dependence of φ on θ_t is linear [cf., Eq. (16)]. However, for α-G*F*E and α-*TE* this function is not linear but it also reaches the value m at $\theta_t = 0$. More interesting is the dependence of φ on $\ln \theta_t$. This dependence is linear at

the region of low absolute values of $\ln \theta_t$. In the region of $\theta_t \to 1$ the following relationship is fulfilled:

$$\varphi = -n \ln \theta_t = n \ln a_0 - n \ln a \tag{19}$$

This relationship may be useful to determine the parameter n from the experimental adsorption data. The dependence of φ on $\ln \theta_t$ is linear at $\theta_t \to 1$ for different values of n, m and α. The lateral interactions ($\alpha > 0$) cause an increase in the values of φ in comparison to the values of φ calculated for $\alpha = 0$. The function φ vs. $\ln \theta_t$ plotted for a greater value of

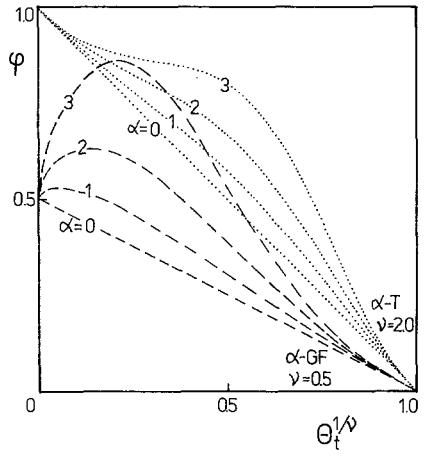

Fig. 3. Dependences φ vs. $\theta_t^{1/\nu}$ for α-G*F* and α-*T* equations with parameters as in Fig. 2

α can have a maximum, whereas this function plotted for $\alpha = 0$ is a decreasing convex curve. Thus, analysing the shape of the experimental function φ vs. $\ln \theta_t$ in comparison to its theoretical behaviour, we can obtain an information about effects due to lateral interactions and energetic heterogeneity of the adsorbent.

In Fig. 2 the dependence of φ^2 on $\ln \theta_t$ is also shown for three main special cases of Eq. (3). This dependence is useful for studying the applicability regions for Eq. (3) and the *Dubinin-Radushkevich* (*DR*) equation[10]. The above problem will be discussed later.

Fig. 3 shows the dependence of φ on $\theta_t^{1/\nu}$ plotted for α-G*F* and α-*T* equations. In the case of the α-*LF*E ($n = m$) this dependence becomes identical with that presented in Fig. 2 A, because $\theta_t^{1/\nu} = \theta_t$. However, in the case of the α-G*F* and α-*T* equations the dependence φ vs. $\theta_t^{1/\nu}$ is linear

for $\alpha = 0$ (cf., Fig. 3), whereas the dependence φ vs. θ_t is not linear even for $\alpha = 0$ (cf., Fig. 2 A). A dominating role of the lateral interactions in the adsorption process may be detected by analysing the experimental curve φ vs. $\theta^{1/\nu}$. If this curve is not linear and lies above the straight line $\varphi = m(1 - \theta_t^{1/\nu})$ [cf., Eq. (16)], it means that the lateral interactions in the surface phase are significant. Moreover, the value of φ at $\theta_t^{1/\nu} = 0$ is

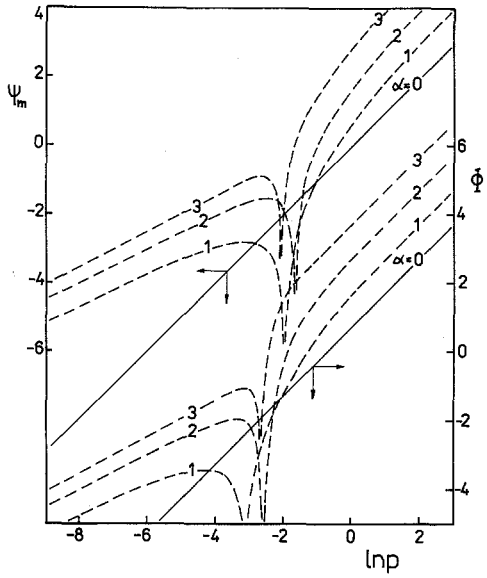

Fig. 4. Functions ψ_m [Eq. (17)] and Φ [Eq. (18)] for α-G*FE* plotted with regard to $\ln p$ for $\bar{K} = 1$ and different values of α. The parameters m and n as in Fig. 2

equal to m. If the value of m is equal to unity for a given adsorption system, it means that this system may be described by a *Tóth*-type equation [Eq. (3) with $m = 1$]. If m is smaller than unity and greater than zero, and $\alpha = 0$, the adsorption system may be described by *LFE* (when φ vs. θ_t is linear) or G*FE* (when φ vs. $\theta_t^{1/m}$ is linear). In the case of $\alpha > 0$ it is difficult to predict on the basis of the dependence φ vs. $\theta_t^{1/\nu}$, which isotherm equation is characteristic for a given adsorption system (α-*LFE* or α-G*FE*).

Figs. 4–6 present the functions ψ_m and Φ vs. $\ln p$ plotted according to Eqs. (17) and (18), respectively. The plots ψ_m and Φ vs. $\ln p$ have been calculated for $n = 1$, $m \in (0,1)$ (α-G*FE*; Fig. 4), $n = m$ (α-*LFE*; Fig. 5),

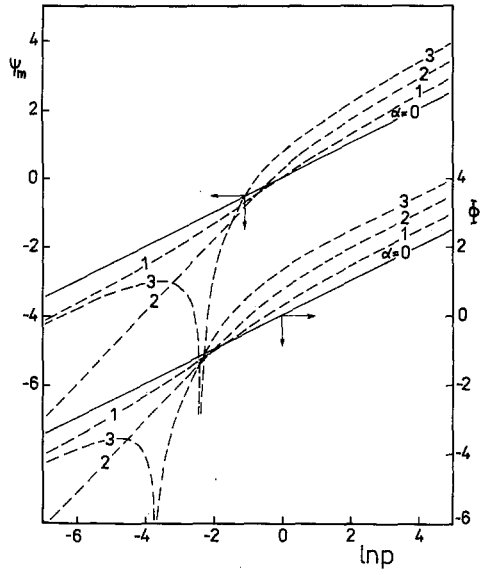

Fig. 5. Functions ψ_m [Eq. (17)] and Φ [Eq. (18)] for α-*LF*E plotted with regard to $\ln p$ for $\bar{K} = 1$ and different values of α. The parameters m and n as in Fig. 2

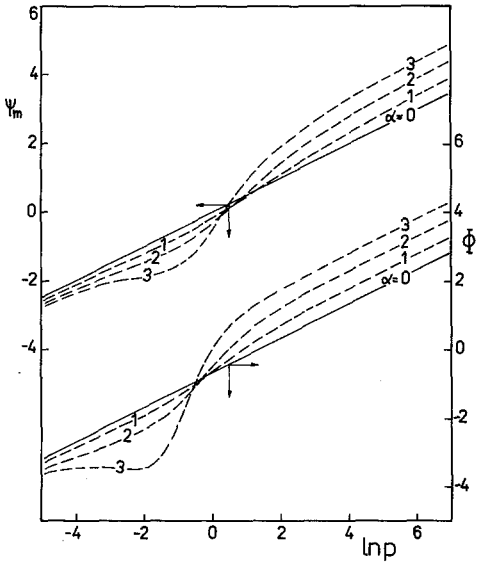

Fig. 6. Functions ψ_m [Eq. (17)] and Φ [Eq. (18)] for α-*T*E plotted with regard to $\ln p$ for $\bar{K} = 1$ and different values of α. The parameters m and n as in Fig. 2

$n \in (0,1)$, $m = 1$ (α-TE; Fig. 6) and different values of α. For $\alpha = 0$ the functions ψ_m and Φ are linear for different values of ν:

$$\Phi = \psi_m - \ln \nu = \ln \left| \frac{\theta_t^{1/\nu}}{\nu (1 - \theta_t^{1/\nu})} \right| = \\ = n \cdot \ln \bar{K} - \ln \nu + n \cdot \ln p \tag{20}$$

The straight lines ψ_m vs. $\ln p$, plotted according to Eq. (20) for different values of n and m, and $\bar{K} = 1$, run across the origin of co-ordinates with the slope equal to n. However, the straight lines Φ vs. $\ln p$, plotted according to Eq. (20), are parallel to the lines ψ_m vs. $\ln p$; the displacement between these lines, calculated along the vertical coordinate is equal to $\ln (1/\nu)$.

The functions ψ_m and Φ vs. $\ln p$, calculated according to Eqs. (17) and (18) for different values of $\alpha > 0$, are parallel to the straight lines plotted according to Eq. (20) in the region of high values of $\ln p$. An increase in the value of α causes only a displacement of the functions ψ_m and Φ in the region of high pressures, whereas their slope is independent on α and equal to n. In the case of α-T equation (Fig. 6) these functions tend asymptotically to the straight lines predicted by Eq. (20) when $\ln p$ tends to minus infinity. It means that their slope at $\ln p \to -\infty$ is also equal to n. However, in the case of α-GF equation at $\ln p \to -\infty$ the functions ψ_m and Φ plotted for different values of α become linear with the slope equal to m. A more complex course of these functions is observed at the values of $\ln p$ belonging to the interval $(-4,2)$. This complex course is caused by the parameter $\alpha > 0$, which characterizes lateral interactions in the surface phase.

It follows from the above discussion of the functions φ, ψ_m and Φ that these functions are very useful to determine the heterogeneity parameters m and n from the experimental adsorption isotherms even if the lateral interactions are significant.

Comparison of G*L Equation with the Dubinin-Radushkevich Isotherm*

The *Dubinin-Radushkevich* (*DR*) isotherm is a very popular equation in the physical adsorption[3,10]. It may be expressed as follows:

$$\theta_t = a/a_0 = \exp \{ - B_0 [RT \ln (p_0/p)^2 \} \quad \text{for} \quad p \leqslant p_0 \tag{21}$$

where B_0 is the heterogeneity parameter, and p_0 is the pressure at which the adsorbed amount is equal to a_0. In the adsorption on microporous solids the pressure p_0 is frequently identified with the saturation vapour pressure p_s (Ref. [10]), although many authors treated p_0 as a

"characteristic" pressure corresponding to the adsorbed amount a_0 (Ref. [3]).

The function φ corresponding to Eq. (21) is expressed as follows:

$$\varphi = 2 B_0 (RT)^2 (\ln p_0 - \ln p) \tag{22}$$

However, the square of φ is equal to:

$$\varphi^2 = 4 \cdot B_0 (RT)^2 (\ln a_0 - \ln a) \tag{23}$$

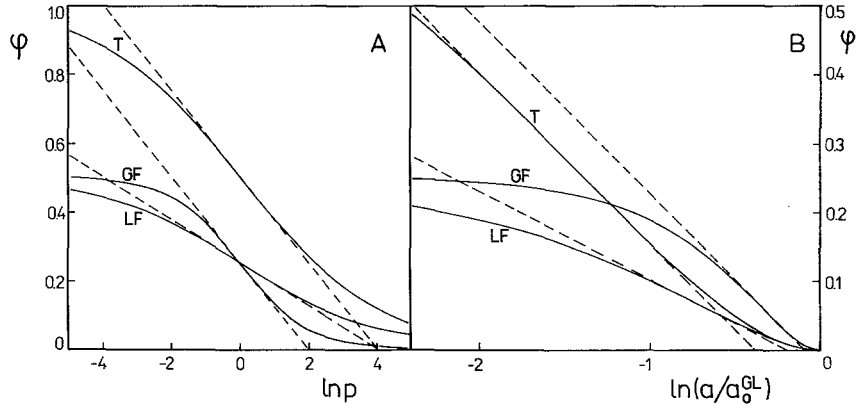

Fig. 7. Comparison of the dependences φ vs. $\ln p$ (part A) and φ^2 vs. $\ln a$ (part B) for the special cases of GL equation (the solid lines; $\bar{K} = 1$, m and n as in Fig. 2) with the DR plots calculated for parameters obtained from Eqs. (27), (28), and (33) (the dashed lines)

Let us compare the functions φ and φ^2, given by Eqs. (22) and (23), with the suitable functions obtained from GL Eq. (1). The function φ corresponding to Eq. (1) is equal to [cf., Eq. (16)]:

$$\varphi = m (1 - \theta_t^{1/v}) \tag{24}$$

As θ_t is the function of pressure p [cf., Eq. (1)], the function φ, Eq. (24), may be plotted in dependence of $\ln p$; such presentation makes the comparison of this function with Eq. (22) easier. The curves $\varphi(\ln p)$ calculated for different values of m and n are decreasing ones with an inflection point (Fig. 7). The coordinates of this point are equal to $\ln p_{in} = -\ln \bar{K}$ and $\varphi_{in} = m/2$.

The region close to the inflection point may be approximated by a straight line. In this region both adsorption isotherms, Eqs. (1) and (21),

may be used to describe the experimental data. The analytical approximation of the function φ given by Eq. (24) may be obtained by expanding Eq. (24) into the *Taylor* series about the point $\ln p_{in}$. Substitution of Eq. (1) into Eq. (24) gives:

$$\varphi = m/[1 + (\bar{K}p)^n] \tag{25}$$

Expanding Eq. (25) into the *Taylor* series about the point $\ln p_{in}$ and neglecting the terms with the second and higher derivatives, we have:

$$\varphi = m/2 + \frac{mn}{4}(-\ln \bar{K} - \ln p) \tag{26}$$

Comparison of Eqs. (22) and (26) gives:

$$B_0 (RT)^2 = mn/8 \tag{27}$$

$$\ln p_0 = 2/n - \ln \bar{K} \tag{28}$$

Eqs. (27) and (28) define the functional dependence between parameters of the DR and GL isotherms in the region in which both equations give a good representation of the experimental adsorption data.

Eq. (27) may be also obtained by comparing Eq. (23) with the analogous function corresponding to the GL isotherm. The function φ^2 relating to Eq. (1) is equal to:

$$\varphi^2 = m^2 \cdot (1 - \theta_t^{1/\nu})^2 \tag{29}$$

This function plotted vs. $\ln \theta_t$, similarily as the function $\varphi(\ln p)$, is a decreasing one with an inflection point of the following coordinates:

$$\ln \theta_{t,in} = -\nu \cdot \ln 2 \tag{30}$$

$$\varphi_{in}^2 = m^2/4 \tag{31}$$

Expanding Eq. (29) into the *Taylor* series about the inflection point $\ln \theta_{t,in}$ and neglecting the terms with the second and higher derivatives, we have:

$$\varphi^2 = m^2/4 + \frac{mn}{2} \cdot (\ln a_0 - \nu \cdot \ln 2 - \ln a) \tag{32}$$

Comparison of Eqs. (23) and (32) gives Eq. (27) and a new equation defining the dependence between the parameters a_0^{GL} and a_0^{DR}; it is:

$$\ln a_0^{DR} = \ln a_0^{GL} + \nu \cdot (0.5 - \ln 2) \tag{33}$$

Thus, Eqs. (27), (28) and (33) give dependences between all parameters of Eqs. (1) and (21). Of course, these equations are valid only in the region of the inflection point of the functions $\varphi(\ln p)$ and $\varphi^2(\ln \theta_t)$ [Eqs. (24) and (29)], in which these functions may be approximated by the straight lines.

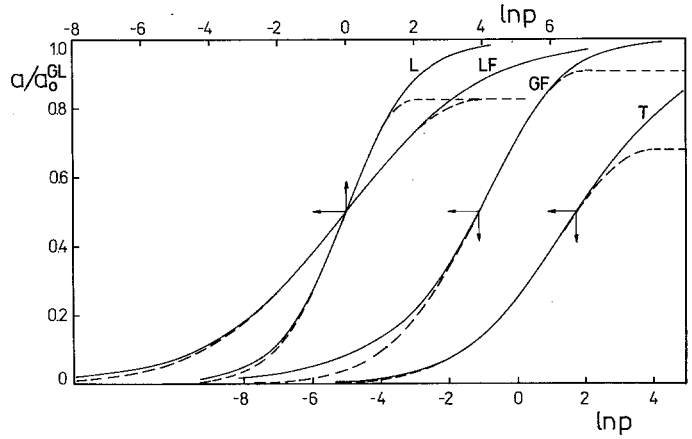

Fig. 8. *DR* Eq. (21) (the dashed lines) and G*L* Eq. (1) (the solid lines) isotherms calculated for the G*L* parameters shown in Figs. 2–7 and the *DR* parameters calculated by means of Eqs. (27), (28), and (33) (as in Fig. 7)

Utilizing these relationships we calculated the *DR* isotherms according to Eq. (21) for different values of m and n (the dashed lines in Fig. 8) in comparison to the suitable G*L* isotherms (the solid lines in this figure). This comparison has been made for the special cases of Eq. (1), i.e., *LE* ($m = n = 1$), *LFE* ($m = n = 0.5$), *GFE* ($m = 0.5$ and $n = 1$) and *TE* ($n = 0.5$ and $m = 1$). It follows from Fig. 8 that the divergence between *DR* and G*L* isotherms appear at low and high pressures. A great divergence between isotherms is observed at the high pressures region; it is caused by the fact that the energy distributions corresponding to *DR* and G*L* isotherms show a most different behaviour at the low adsorption energies corresponding to high pressures. This effect is shown in Fig. 9, in which the energy distribution functions relating to *DR* and G*L* isotherms obtained by using the condensation approximation method[11] are compared. Equations for the energy distributions corresponding to the *DR* and G*L* isotherms may be derived by means of the well-known relationship[11]:

$$F_c(\varepsilon) = -\frac{\mathrm{d}\theta_t(p(\varepsilon))}{\mathrm{d}\varepsilon} \tag{34}$$

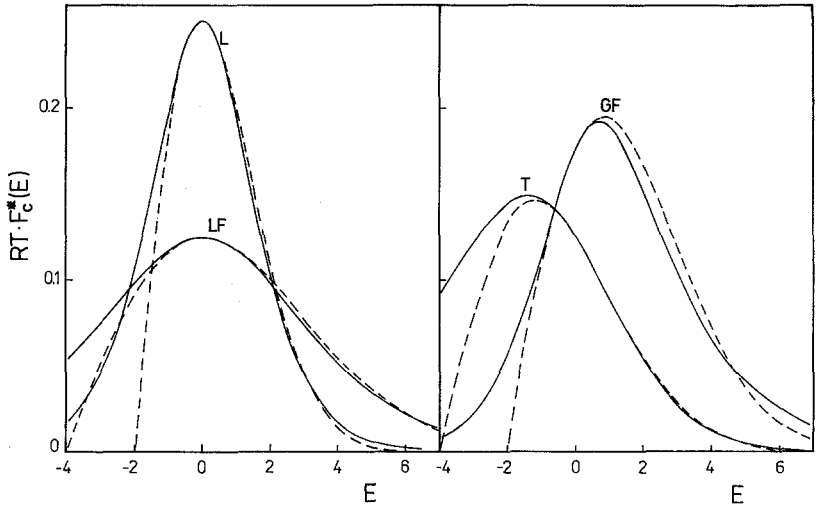

Fig. 9. Energy distributions obtained by using the condensation approximation method for the G*L* Eq. (38) and parameters shown in Figs. 7 and 8 (the solid lines) and for the *DR* Eq. (37) with parameters obtained from Eqs. (27), (28), and (33) (the dashed lines)

where

$$\varepsilon(p) = -RT\ln(K_0 p) \tag{35}$$

Let us define the energy ε_0 for the *DR* and G*L* equations by

$$\varepsilon_0 = \begin{cases} -RT\cdot\ln(K_0 p_0) & \text{for Eq. (21)} \\ RT\cdot\ln(\bar{K}/K_0) & \text{for Eq. (1)} \end{cases} \tag{36}$$

Equations defining the energy distributions for Eq. (1) and (21), obtained by means of Eqs. (34), (35), and (36), are expressed as follows:

$$F_c(RTE + \varepsilon_0) = F_c^*(E) = \\ = 2\cdot B_0 RTE\cdot\exp[-B_0(RTE)^2] \quad \text{for Eq. (21)} \tag{37}$$

and

$$F_c(RTE + \varepsilon_0) = F_c^*(E) = \\ = \frac{m}{RT}\exp(nE)\cdot[1+\exp(nE)]^{-(\nu+1)} \quad \text{for Eq. (1)} \tag{38}$$

where

$$E = (\varepsilon - \varepsilon_0)/RT \tag{39}$$

The DR energy distribution is equal to zero at $\varepsilon = \varepsilon_0$ and tends asymptotically to zero when $\varepsilon \to \infty$. However, the energy distributions calculated according to Eq. (38) for different values of m and n tends asymptotically to zero for ε tending to minus or plus infinity. Therefore, a great divergence between DR and GL distributions appears at low adsorption energies, which correspond to high pressures. At high adsorption energies a best coincidence of the energy distributions is observed for $m = 1$ and $n \in (0,1)$, whereas this coincidence for $m \in (0,1)$ and $n = 1$ is poor. In the region of the maximum the best coincidence between DR and GL energy distributions is observed for $m = n$. It follows from comparison of the energy distributions presented in Fig. 9 that a greatest region of coincidence is observed for DR and LF energy distributions. This conclusion is in an excellent agreement with the studies of *Dubinin*[12—14], who showed that the DR adsorption isotherm and the LF isotherm ($n = m$) are equivalent at a wide region of surface coverages. The TE isotherm shows also an excellent coincidence to the DR one in the region of high adsorption energies, but their similarity is limited by the very poor coincidence in the region of low energies. However, for GF and DR equations coincidence is better for the low energies region, than that for LFE and TE ones, but is very poor for the high adsorption energies region.

Application of GLE *for Analysing Gas Adsorption Data*

For the purpose of illustration we applied Eq. (1) for describing the adsorption of argon on porous silver at 77.4 K[15] and nitrogen on silica gel at 77.4 K[16]. The above experimental data were analysed by means of Eq. (1) with the BET multilayer correction, i.e.:

$$\theta_t = \frac{1}{1-x}\left[\frac{(\bar{C}x)^n}{1+(\bar{C}x)^n}\right]^{\nu}; \quad \bar{C} = \bar{K}p_s \tag{40}$$

Fig. 10 presents the linear dependence $[(1-x)a]^{1/\nu}$ vs. $[(1-x)a]^{1/\nu}x^{-n}$ for adsorption data of argon on porous silver plotted according to the following relationship:

$$[(1-x)a]^{1/\nu} = a_0^{1/\nu} - (\bar{C})^{-n}[(1-x)a]^{1/\nu}x^{-n} \tag{41}$$

The parameter n has been evaluated by means of the function ψ_1 [Eq. (20) with $m = 1$]; because this function calculated from the

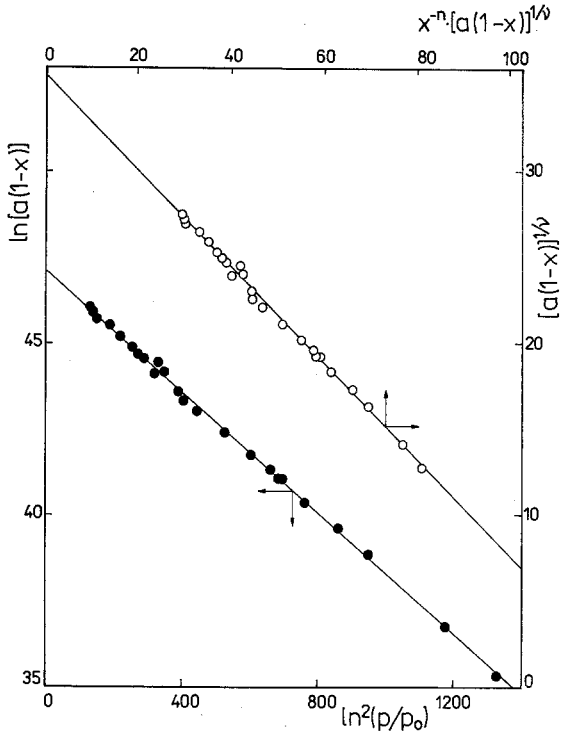

Fig. 10. Linear dependences plotted according to Eqs. (41) (the white circles) and (42) (the black circles) for adsorption data of argon on porous silver at 77.4 K[15]. The parameters were taken from Table 1 and a is expressed in number of atoms

experimental data is linear, the parameter n could be evaluated from its slope. This parameter and the parameters a_0, $\overline{C}$ and p_s are summarized in Table 1.

The same data have been plotted according to the linear form of *DR* Eq. (21) with the *BET* multilayer correction, it is

$$\ln[a(1-x)] = \ln a_0 - B_0(RT)^2[\ln(p/p_0)]^2 \tag{42}$$

The linear dependence $\ln[a(1-x)]$ vs. $[\ln(p/p_0)]^2$ is presented in Fig. 10. The parameter p_0 has been evaluated by means of the functions φ plotted according to Eq. (22). However, the parameters a_0 and $B_0(RT)^2$ were calculated according to Eq. (42) and are also given in Table 1. It follows from Fig. 10 and Table 1 that both isotherm equations, *DR* and *Tóth* (*GL* with $m = 1$), give a good representation of

Table 1. *Parameters characterizing the adsorption of argon on porous silver at 77.4 K (Ref.* [15]*) and nitrogen on silica gel at 77.4 K (Ref.* [16]*)*

System	$\ln p_s$ [Torr]	GL parameters m	n	$\ln \bar{K}$ [Torr^{-1}]	$\ln a_0$	DR parameters $B_0(RT)^2 \cdot 10^2$	$\ln p_0$ [Torr]	$\ln a_0$	DR parameters calculated from Eqs. (27), (28), (33) $B_0(RT)^2 \cdot 10^2$	$\ln p_0$ [Torr]	$\ln a_0$
Ar/porous silver	5.35	1.0	0.072	12.45	49.6*	0.88	16.0	47.1*	0.90	15.3	46.9*
N_2/silica gel	6.64	1.0	0.197	6.54	1.94**	1.74	6.64	1.50**	2.46	3.61	0.96**

* [atoms].
** [mmol/g].

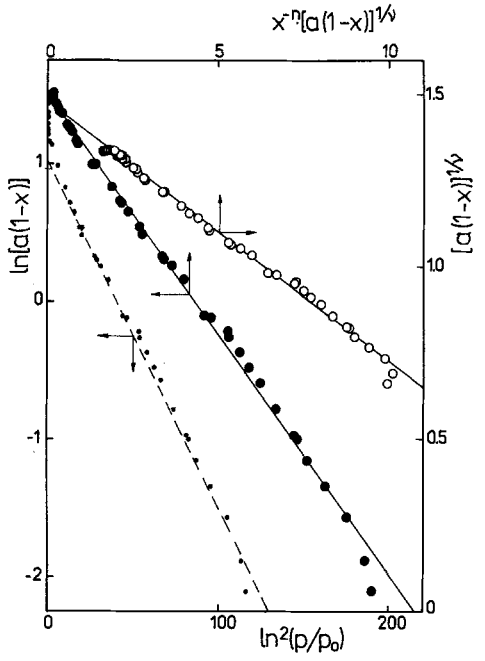

Fig. 11. Linear dependences plotted according to Eqs. (41) (the white circles) and (42) (the black circles and black points) for adsorption data of nitrogen on silica gel at 77.4 K[16]. The straight dashed line with the black points was calculated by using the parameters obtained from Eqs. (27), (28), and (33), whereas the solid line with the black circles was plotted for the best fit parameters obtained from φ vs. $\ln p$ (see Table 1 and Fig. 12). The adsorbed amount is expressed in mmol/g

the argon adsorption data on porous silver. Nevertheless, the parameter p_0 evaluated by means of Eq. (22) is not equal to p_s for argon at 77.4 K. It means that although the *DR* equation fulfills the argon adsorption data on porous silver, the mechanism of adsorption in this system is analogous as in the case of adsorption on wide-porous solids[17]. It follows from the studies of *Dubinin*[10] that in the case of micropore filling the parameter p_0 appearing in his equation is frequently identified with p_s or it is close to p_s.

Quite similarily as in the case of argon adsorption, the nitrogen adsorption data on silica gel at 77.4 K were analysed by using *DR* and *Tóth* (*GLE* with $m = 1$) equations.

Fig. 11 presents the dependences (41) and (42) for this adsorption system. However, Table 1 contains the parameters characterizing the

nitrogen adsorption on silica gel. In this case the parameters p_0 and p_s are similar; thus, the mechanism assuming pore filling is more probable.

Table 1 contains also the parameters a_0, $B_0 (RT)^2$ and p_0 evaluated by means of Eqs. (27), (28), and (33). In the case of argon adsorption on porous silver the parameters a_0, $B_0 (RT)^2$, and p_0, evaluated by means of the linear dependence Eq. (42) and calculated according to Eqs. (27), (28), and (33), are very similar. However, in the case of nitrogen

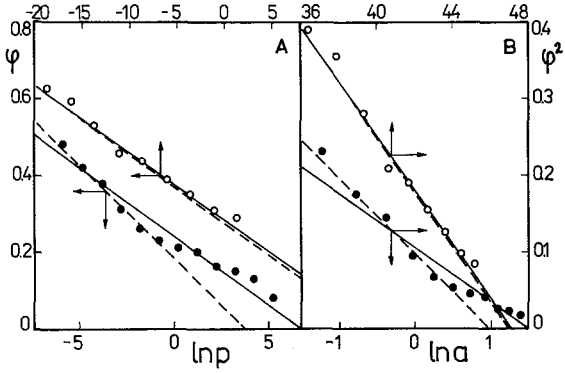

Fig. 12. The *DR* equation linear dependences φ vs. $\ln p$ (part A) and φ^2 vs. $\ln a$ (part B) plotted according to adsorption data of argon on porous silver at 77.4 K[15] (the solid lines with the white circles) and nitrogen on silica gel at 77.4 K[16] (the solid lines with the black circles). The dashed lines refer to the *DR* parameters obtained from G*L*E parameters by using relations (27), (28), and (33) (see Table 1)

adsorption data on silica gel, their similarity is worse. In the first case the adsorption data were measured at the pressure region about the inflection point of the function φ ($\ln p$). In this region Eqs. (27), (28), and (33) are valid. However, the region of nitrogen adsorption data is shifted in the direction of higher pressures, in which the linear approximation of φ ($\ln p$) corresponding to G*L* equation is worse (cf., solid lines in Fig. 12). In Fig. 12 A the functions φ ($\ln p$) are presented and in Fig. 12 B the dependence φ^2 ($\ln a$) are shown for the both systems discussed above. For comparison are also shown the straight lines obtained for *DR* equation parameters calculated from G*L*E parameters (the dashed lines in Fig. 12).

In Fig. 11 is also shown the dependence (42) (the black points and the dashed line) obtained for the parameters calculated by means of Eqs. (27), (28), and (33) and presented in Table 1.

Therefore, the parameters $B_0 (RT)^2$, a_0 and p_0 calculated according to Eqs. (27), (28), and (33) differ from those evaluated by means of Eq. (42).

Nevertheless, we can write three inequalities, corresponding to Eqs. (27), (28), and (33), which determine the direction of changes of these parameters when the region of the available adsorption data lies far from the inflection point of the function $\varphi (\ln p)$. They are:

$$B_0 (RT)^2 \leqslant mn/8 \tag{43}$$

$$\ln a_0^{DR} \geqslant \ln a_0^{GL} - 0.193 \cdot \nu \tag{44}$$

$$\ln p_0 \geqslant 2/n - \ln \bar{K} \tag{45}$$

It follows from Table 1 that the parameters $B_0 (RT)^2$, a_0^{DR} and p_0 calculated according to Eqs. (27), (28), and (33) and evaluated by means of Eq. (42), satisfy these inequalities.

Extension of GLE to Gas Adsorption on Heterogeneous Surfaces Characterized by More Complex Energy Distributions

The energy distributions characterizing many real adsorption systems show complex behaviour[18–20] and they can not be approximated by simple equations which are obtained from *DR* and *GL* adsorption isotherms. This means that many real adsorption systems do not fulfil *DR* and *GL* equations in a wide pressure range. However, these systems may be described by the isotherm equations being a linear combination of the simple adsorption isotherms, i.e.:

$$\theta_t = \sum_{i=1}^{r} f_i \theta_{t,i} \tag{46}$$

where

$$f_i = a_{0i}/a_0 \tag{47}$$

Then the energy distribution function corresponding to Eq. (46) is a linear combination of the simple energy distributions relating to $\theta_{t,i}$, i.e.:

$$F(\varepsilon) = \sum_{i=1}^{r} f_i \cdot F_i(\varepsilon) \tag{48}$$

Figs. 13 A and C show the energy distributions being a sum of the distributions corresponding to *Tóth* and *GF* equations. These distributions have been calculated for different parameters m_i, n_i and ε_{0i} according to the equation derived in the previous paper[1]. The subscript

"i" refers to the i-th simple energy distribution. However, Figs. 13 B and D present the functions ψ_m, ψ_1 and Φ calculated for the following theoretical adsorption isotherms:

$$\theta_t = 0.7\left(\frac{10p}{1+10p}\right)^{0.5} + 0.3\left(\frac{p^{0.5}}{1+p^{0.5}}\right)^2 \tag{49}$$

$$\theta_t = 0.7\left(\frac{p}{1+p}\right)^{0.5} + 0.3\left[\frac{(10p)^{0.5}}{1+(10p)^{0.5}}\right]^2 \tag{50}$$

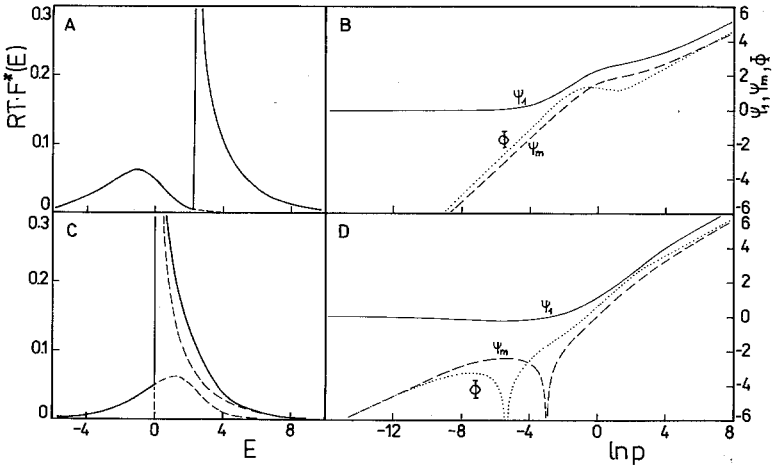

Fig. 13. The total energy distributions (the solid lines) refering to the isotherms given by Eq. (49) (part A) and Eq. (50) (part C) with their partial distributions (the dashed lines) and corresponding functions Φ (the dotted lines), ψ_m (the dashed lines) and ψ_1 (the solid lines) plotted with respect to $\ln p$ (parts B, D)

As it has been shown in Figs. 4 and 6, the functions ψ_m and Φ corresponding to the *Tóth* and *GF* equations ($\alpha = 0$) are linear. However, these functions calculated for the adsorption isotherm given by Eq. (46) are not linear. Nevertheless, if the adsorption isotherm corresponds to the energy distribution composed from well separated simple distributions Fig. 13 A, the functions ψ_m and Φ have linear segments, from which the heterogeneity parameters may be evaluated. In Fig. 13 the function ψ_1 is also shown. This function may be useful to determine the parameter n at the region of high pressures.

To illustrate the utility of the overall adsorption isotherm given by Eq. (46) we analysed the argon adsorption data on rutile at 85 K[21]. These data were measured with a great precision[21] and were used by many

authors to examine the methods for determining the energy distribution function[22–26]. Our studies showed that these adsorption data may be approximated by the following equation:

$$a(1-x) = a_{01}\left\{\frac{[\bar{C}_1 h(x)]^{n_1}}{1+[\bar{C}_1 h(x)]^{n_1}}\right\}^{\left(\frac{m_1}{n_1}\right)} + a_{02}\left\{\frac{[\bar{C}_2 h(x)]^{n_2}}{1+[\bar{C}_2 h(x)]^{n_2}}\right\}^{\left(\frac{1}{n_2}\right)} \tag{51}$$

where $h(x)$ is defined by Eq. (6). The adsorption isotherm given by Eq. (51) takes into account the *BET* multilayer correction. The first term of Eq. (51) represents the general form of G*L*E, whereas the second term represents its special form, i.e., *Tóth* equation (G*L*E with $m = 1$). The parameters of Eq. (51) were evaluated as follows: first of all, the function $\varphi(\ln p)$ has been calculated from argon adsorption data on rutile. Its shape indicates an existence of two main groups of adsorption sites (cf., Fig. 14). This conclusion is in a good agreement with studies of *Oh* and *Kim*[25], *Aston* et al.[26] and *Rudziński* and *Jaroniec*[23], who found three groups of adsorption sites. According to these studies[23,25,26] the number of adsorption sites of the third group is small in comparison to the number of remaining sites. Therefore, the function $\varphi(\ln p)$ makes possible only the detection of two main groups of adsorption sites. The function $\Phi(\ln p)$ (see Fig. 14) has been calculated by means of $\varphi(\ln p)$. According to Eq. (20) we evaluated the heterogeneity parameter n_1 from the linear segment of $\Phi(\ln p)$ in the region of high pressures, which corresponds to the region of low adsorption energies. Knowing the parameter n_1, the parameters m_1, $\bar{C}_1$ may be evaluated by using the linear segment of the dependence $(1/\varphi)$ vs. $[h(x)]^n$ in the region of high pressures:

$$(1/\varphi) = (1/m) + [h(x)]^n \cdot (\bar{C})^n/m \tag{52}$$

The parameter a_{01} and also the parameter $\nu = m/n$ may be evaluated by using the linear segment of the dependence $\ln a$ vs. $\ln\{1 + [\bar{C} \cdot h(x)]^{-n}\}$ in the region of high pressures:

$$\ln a = \ln a_0 - \ln\{1 + [\bar{C} \cdot h(x)]^{-n}\} \tag{53}$$

Knowing the parameters a_{01}, $\bar{C}_1$, n_1, m_1, evaluated from the high pressure adsorption data, we can calculate the adsorption a_1 according to the first term of Eq. (51). The adsorption a_2, occuring on sites of the second group may be calculated as follows [cf., Eq. (51)]:

$$a_2 = a \cdot (1-x) - a_1 \tag{54}$$

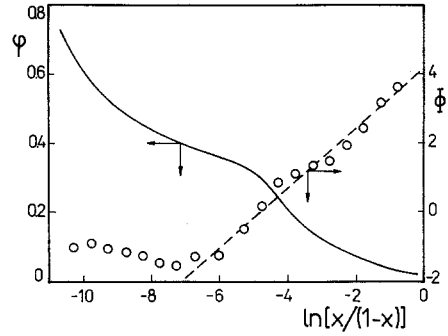

Fig. 14. Function φ vs. $\ln[x/(1-x)]$ (the solid line) and Φ vs. $\ln[x/(1-x)]$ (the white circles) with the straight line approximation in the region of high pressures (the dashed line) for the argon adsorption data on rutile at 85 K[21]

Table 2. *Parameters characterizing the adsorption of argon on rutile at 85 K (Ref.* [21]*) [Eq. (51)]*

i	a_{0i}^*	$\bar{C}_i$	m_i	n_i
1	630	70	0.60	0.88
2	139	13 200	1.00	0.56

* Total $a_0 = 769\ \mathrm{cm^3/g}$, whereas a_0 evaluated by *Dormant* and *Adamson*[22] is equal to $755\ \mathrm{cm^3/g}$; the saturation pressure $p_s = 592$ Torr.

The parameters a_{02}, $\bar{C}_2$, n_2 and m_2 may be evaluated from the adsorption data a_2 vs. x by using the same procedure as it is described above. The adsorption parameters, evaluated for this system, are summarized in Table 2. However, Fig. 15 presents the theoretical adsorption isotherm, calculated according to Eq. (51) by using parameters from Table 2, in comparison to the experimental one. This figure shows also the total energy distribution $F(\varepsilon)$ calculated according to Eq. (48), and for comparison it also shows that calculated by *Dormant* and *Adamson*[22]. Our function is slightly shifted in the direction of low adsorption energies in comparison to the distribution evaluated by *Dormant* and *Adamson*[22]. The position of energy distribution on the energy axis depends on K_0; our function has been plotted for K_0 evaluated by *Dormant* and *Adamson*[22]. However, the courses of both distributions are similar. Assumption of two subsurfaces (two groups of adsorption sites),

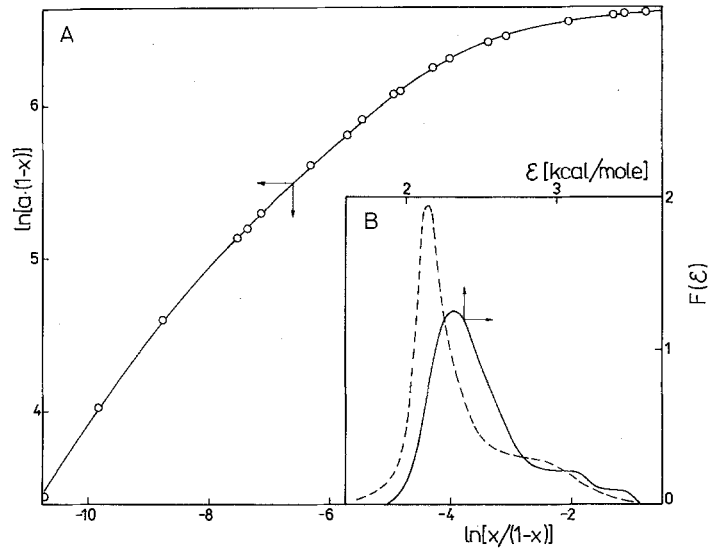

Fig. 15. The dependence $\ln[a(1-x)]$ vs. $\ln[x/(1-x)]$ (the white circles) in comparison to the theoretical curve plotted according to parameters summarized in Table 2 (part A) and energy distributions $F(\varepsilon)$ vs. ε plotted according to *Dormant* and *Adamson*[22] (the solid line in part B) and according to our approximate evaluation (the dashed line in part B) for the argon adsorption data on rutile at 85 K[21]. The adsorbed amount is expressed in [cm^3/g] and $F(\varepsilon)$ in [$mol/(cal \cdot cm^3)$][21,22]

characterized by energy distributions $F_1(\varepsilon)$ and $F_2(\varepsilon)$ respectively, is already sufficient to reflect the main features of the real energy distribution.

Concluding Remarks

The energy distribution of *Tóth*-type [$m = 1$ and $n \in (0,1)$] is less realistic from the physical viewpoint, because it is extended in the direction of low adsorption energies[9]. However, the majority of real gas/solid adsorption systems are characterized by quasi-*Gaussian* energy distribution extended in the direction of high adsorption energies[18—20]. Such distributions are generated by GL equation for $n > m$. The main disadvantage of the distributions of GL-type with $n > m$ and $n \in (0,1)$ is their behaviour at very high adsorption energies. They decrease too much slowly in the region of highest energies. However, they give a good representation of the real energy distributions at the moderate and lower adsorption energies. In contrast

to it the *Tóth*-type distribution approximates well the real energy distributions at highest adsorption energies. This distribution, although it does not predict the maximum adsorption energy assuming the *Henry* behaviour at very low pressures, decreases sufficiently fast at highest adsorption energies and in consequence gives Henry's law at very low pressures. Therefore, the *Tóth*-type equation [GL equation with $m = 1$ and $n \in (0,1)$] is frequently used to describe the experimental adsorption systems. Nevertheless, approximation of the real energy distribution by means of the *Tóth*-type distribution is possible only then, when the parameter $a_0^{Tóth}$ is considerably greater than the real value of a_0 (e.g., a_0 predicted by the *BET* method). It is illustrated in Fig. 9, which shows that the real non-normalized function $F_n(\varepsilon)$ (in that figure it is *DR* one), may be approximated by the non-normalized *Tóth*-type function $F_n^T(\varepsilon)$ satisfying the following inequality:

$$a_0^T = \int_\Delta F_n^T(\varepsilon) \cdot d\varepsilon > a_0 = \int_\Delta F_n(\varepsilon)\, d\varepsilon \tag{55}$$

The values a_0^T obtained by the *Tóth* isotherm from the experimental adsorption data are usually greater than a_0 predicted by the *BET* method and other equations, such as *LF* and *DR* equations[27,28]; it confirms our considerations leading to the inequality (55). The effects of lateral interactions and multilayer effects may cause an extension of the evaluated energy distribution in the direction of lower adsorption energies[29,30]. Thus, these effects cause an elevation of the adsorption isotherm at high pressures in comparison to that predicted by a monolayer isotherm corresponding to the real energy distribution. However, the adsorption data perturbed by lateral interactions and multilayer effects are frequently well approximated by the simple *Tóth* equation [Eq. (1) with $m = 1$]. Then we obtain the *Tóth*-type energy distribution which does not coincide with the real distribution at low adsorption energies. This divergence between the calculated and real distributions may be caused by multilayer effects and lateral interactions in the monolayer. Therefore, the determination of heterogeneity effects by using the experimental adsorption data is very difficult. Nevertheless, a complex analysis of the adsorption data by means of different isotherm equations and thermodynamic tests makes it possible to select a correct adsorption isotherm reflecting the physical properties of the real adsorption system.

References

[1] Part I: *Jaroniec M., Marczewski A. W.*, Monatsh. Chem. **115**, 997 (1984).
[2] *Marczewski A. W., Jaroniec M.*, Monatsh. Chem. **114**, 711 (1983).
[3] *Jaroniec M.*, Advances in Colloid and Interface Sci. **18**, 149 (1983).

[4] *Berezin G. J., Kiselev A. V.*, J. Colloid Interface Sci. **46**, 203 (1974).
[5] *Jaroniec M., Rudziński W.*, Acta Chim. Hung. **88**, 351 (1976).
[6] *Dubinin M. M., Jakubov T. S., Jaroniec M., Serpinsky V. V.*, Polish J. Chem. **54**, 1721 (1980).
[7] *Misra D. N.*, J. Chem. Phys. **52**, 5499 (1970).
[8] *Garbacz J. K., Jaroniec M., Deryło A.*, Thin Solid Films **75**, 307 (1981).
[9] *Tóth J., Rudziński W., Waksmundzki A., Jaroniec M., Sokołowski S.*, Acta Chim. Hung. **82**, 11 (1974).
[10] *Dubinin M. M.*, Progress in Surface and Membrane Sci. **9**, 1 (1975).
[11] *Cerofolini G. F.*, Thin Solid Films **23**, 129 (1974).
[12] *Jakubov T. S., Bering B. P., Dubinin M. M., Serpinsky V. V.*, Izv. Akad. Nauk SSSR, Ser. Khim. **77**, 463 (1977).
[13] *Dubinin M. M., Jakubov T. S.*, Izv. Akad. Nauk SSSR, Ser. Khim. **77**, 2428 (1977).
[14] *Dubinin M. M.*, Izv. Akad. Nauk SSSR, Ser. Khim. **78**, 529 (1978).
[15] *Hobson J. P.*, J. Phys. Chem. **73**, 2720 (1969).
[16] *Drieving V. P., Kiselev A. V., Lichaczieva O. A.*, Zh. Fiz. Khim. **25**, 709 (1951).
[17] *Dubinin M. M.*, in: Adsorption—Desorption Phenomena, p. 3. New York: Academic Press. 1972.
[18] *Jaroniec M.*, Surface Sci. **50**, 553 (1975).
[19] *House W. A.*, in: Specialist Periodical Reports. Colloid Science (*Everett D. H.*, ed.), Vol. **4**, ch. 1. London: Chem. Soc.
[20] *Zolandz R. R., Myers A. L.*, Progress in Filtration and Separation Sci., Vol. 1, pp. 1—29. Amsterdam: Elsevier. 1979.
[21] *Drain L. E., Morrison J. A.*, Trans. Faraday Soc. **48**, 840 (1952).
[22] *Dormant L. H., Adamson A. W.*, J. Colloid Interface Sci. **38**, 285 (1972).
[23] *Rudziński W., Jaroniec M.*, Surface Sci. **42**, 552 (1974).
[24] *Jaroniec M., Rudziński W.*, Colloid and Polymer Sci. **253**, 683 (1975).
[25] *Oh K., Kim S. K.*, J. Chem. Phys. **67**, 3416 (1977).
[26] *Aston J. G., Tykodi R. J., Steele W. A.*, J. Phys. Chem. **59**, 1053 (1955).
[27] *Rudziński W., Jaroniec M., Łajtar L.*, Wiadom. Chem. (Poland) **30**, 305 (1976).
[28] *Tóth J.*, Proc. Int. Conf. Colloid and Surface Sci. (*Wolfram E.*, ed.), p. 41. Budapest: Akadémiai Kiadó. 1975.
[29] *Bräuer P., House W. A., Jaroniec M.*, Thin Solid Films **97**, 369 (1982).
[30] *Bräuer P., House W. A., Jaroniec M.*, Wiss. Z. FS Univ. Jena, Math.-Naturwiss. R. **31**, 987 (1982).